Contents lists available at SciVerse ScienceDirect

Chemical Engineering Research and Design

journal homepage: www.elsevier.com/locate/cherd

Effect of oscillation amplitude on velocity distributions in an oscillatory baffled column (OBC)

Ahmad Azahari Hamzah[a], *Nurul Hasan*[b,*], *Mohd Sobri Takriff*[a], *Siti Kartom Kamarudin*[a], *Jaafar Abdullah*[c], *Isa M Tan*[b], *Wah Keng Sern*[a]

[a] *Department of Chemical & Process Engineering, Faculty of Engineering & Built Environment, National University of Malaysia, 43600 Bangi, Malaysia*

[b] *Department of Chemical Engineering, University Technology Petronas, Bandar Seri Iskandar, 31750 Tronoh, Malaysia*

[c] *Centre of Computed Tomography and Industrial Imaging, Malaysia Nuclear Agency, Bangi, 43000 Kajang, Selangor, Malaysia*

ABSTRACT

This paper presents a numerical study of the effect of oscillation amplitude in oscillatory baffled column (OBC) using computational fluid dynamics. The numerical work was carried out for single phase liquid flow for an unsteady 3-D model using commercial software, Fluent (2006). This work was concentrated on the effect of oscillation amplitude. Three amplitudes of 5, 10 and 15 mm with constant frequency of 1 Hz are applied. Vortex and cycle average velocities at different points are analyzed. The studies show the maximum velocity for 5 mm, 10 mm and 15 mm in an OBC are 0.11 m/s, 0.25 m/s and 0.40 m/s respectively in the first cycle of oscillation. At a constant frequency, greater oscillation amplitude displaces the liquid to a further distance and builds a larger vortex. Vortex length was 1.5 times bigger when oscillation amplitude changes from 5 mm to 10 mm and 2 times when the amplitude is triple from 5 mm. The detailed validation is presented somewhere else; this research is focused on the effect of oscillation.

Keywords: CFD; Flow pattern; Oscillatory baffled column; Oscillation amplitude; Vortex length; Velocity distributions

1. Introduction

Mixing has great importance in chemical and biochemical industries. Basic phenomenon for mixing enhancement is the production of cyclic discrete vortices in the bulk fluid (Ni et al., 2003a). Oscillatory baffled column (OBC) is a device that can enhance the formation of vortices and increase the intensity of mixing process. Previous studies showed that OBC successfully increases mass transfer (Stonestreet and Harvey, 2002), heat transfer (Mackley and Stonestreet, 1995), chaotic mixing (Reis et al., 2004) and residence time (Stephens and Mackley, 2002) compared to other mixing equipments. It can be operated in batch or continuous mode depending on the process itself. The key feature of oscillating baffled flows is that mixing can be controlled to a very high degree of precision, giving a wide range of mixing conditions, from 'soft' mixing, exhibiting plug flow characteristics, to the most intense, approaching mixed flow conditions (Ni et al., 2003b). OBC is widely used in laboratory scale to industrial applications such as photocatalytic wet oxidation (Fabiyi and Skelton, 1999), polymerisation processes (Ni et al., 2002b) and heterogeneous photocatalytic oxidation (Gao et al., 2003). A typical experimental set is shown in Fig. 1 as performed in the current investigation.

With the rapid advancement in computational fluid dynamics (CFD) modeling, studying local flow and transport phenomena in OBC has become feasible. Various aspects of the study were conducted on the OBC using the CFD such as effect of viscosity (Fitch et al., 2005), flow dynamics (Ni et al., 2002a), scale up behavior (Jian and Ni, 2005), effect of gap between baffle and wall (Ni et al., 2004) and shear rate distributions (Reis et al., 2004). These studies show that an OBC has capabilities to increase the intensity of mixing.

The dynamics in an OBC is controlled by dimensionless parameters which are Reynolds number ($Re_n = uD/v = uD\rho/\mu$), oscillatory Reynolds number ($Re_o = u_oD/v = x_o\omega D\rho/\mu = 2\pi f x_o \rho D/\mu$), and the Strouhal number ($S_t = D/4\pi x_o$).

* *Corresponding author*. Tel.: +60 5 368 7638; fax: +60 5 365 6176.
E-mail address: nurul_hasan@petronas.com.my (N. Hasan).

Received 1 December 2010; Received in revised form 11 September 2011; Accepted 4 November 2011
0263-8762/$ – see front matter
doi:10.1016/j.cherd.2011.11.003

Nomenclature

$Re_n = uD/v = uD\rho/\mu$ Reynolds number
$Re_o = u_oD/v = x_o\omega D\rho/\mu = 2\pi f x_o \rho D/\mu$ oscillatory Reynolds number
$S_t = D/4\pi x_o$ Strouhal number
D diameter of column, m
f oscillation frequency, Hz
p pressure drop, Pa
t time, s
u velocity, m/s
V_r, V_θ, V_z laminar velocity velocities (m/s) at r, θ_v and z coordinates
x_o oscillation amplitude, m
x co-ordinates in x direction, m
y co-ordinates in y direction, m
z co-ordinates in z direction, m

Greek letters
μ fluid viscosity, kg/ms
μ_o nominal laminar viscosity, kg/ms
μ_t turbulent viscosity, kg/ms
ρ fluid density, kg/m^3
τ shear stress, N/m^2
ν the kinematic viscosity of fluid, m^2/s

Oscillatory Reynolds numbers represents the intensity of mixing applied to column. Strouhal number represents the ratio of column diameter to amplitude length, measuring the effective eddy propagation (Ni and Gough, 1997). In the previous studies, the effect of S_t is lacking. This paper will reveal the effect of S_t. After the computational model in the next section, the results and conclusions are presented.

Fig. 1 – An experimental set up for the OBC.

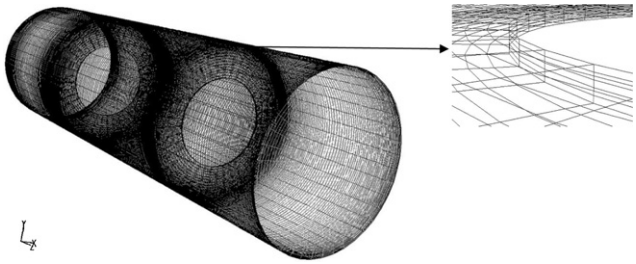

Fig. 2 – Grid view for 3-D model.

2. Computational models

All the models were three-dimensional and considered incompressible and laminar. The governing equations in cylindrical coordinates for continuity and momentum (Ni et al., 2002a; Jian and Ni, 2005) are as follows:

Continuity equations:

$$\frac{1}{r}\frac{\partial}{\partial r}(rV_r) + \frac{1}{r}\frac{\partial V_\theta}{\partial \theta} + \frac{\partial V_z}{\partial z} = 0 \quad (1)$$

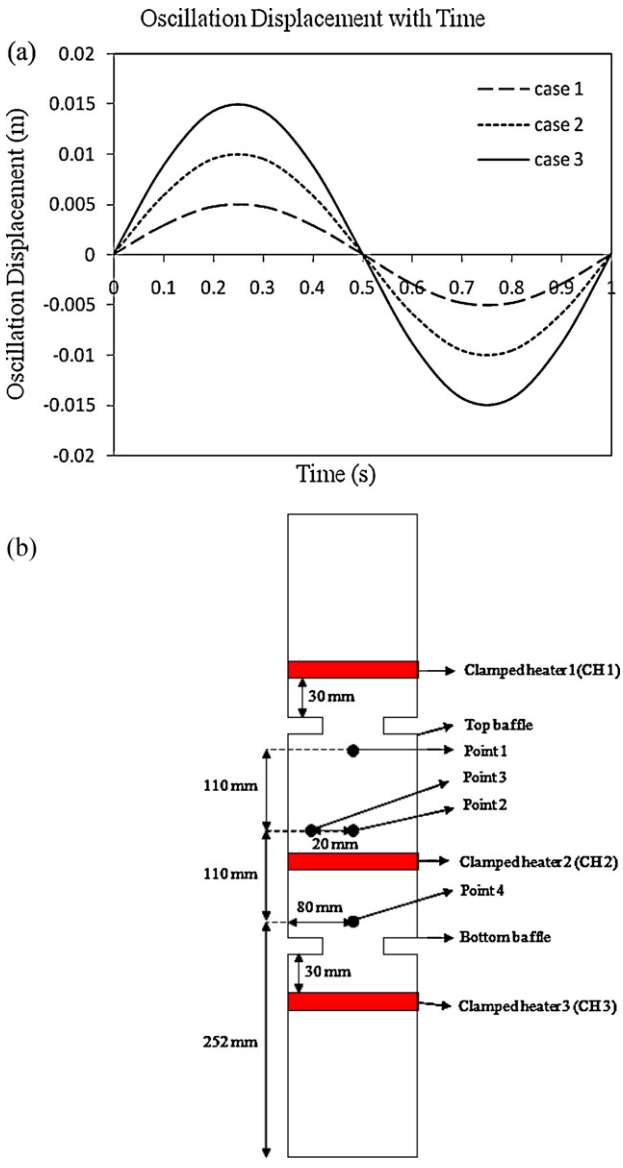

Fig. 3 – Oscillation displacement with time for test cases (Table 1). (b) Focus point locations.

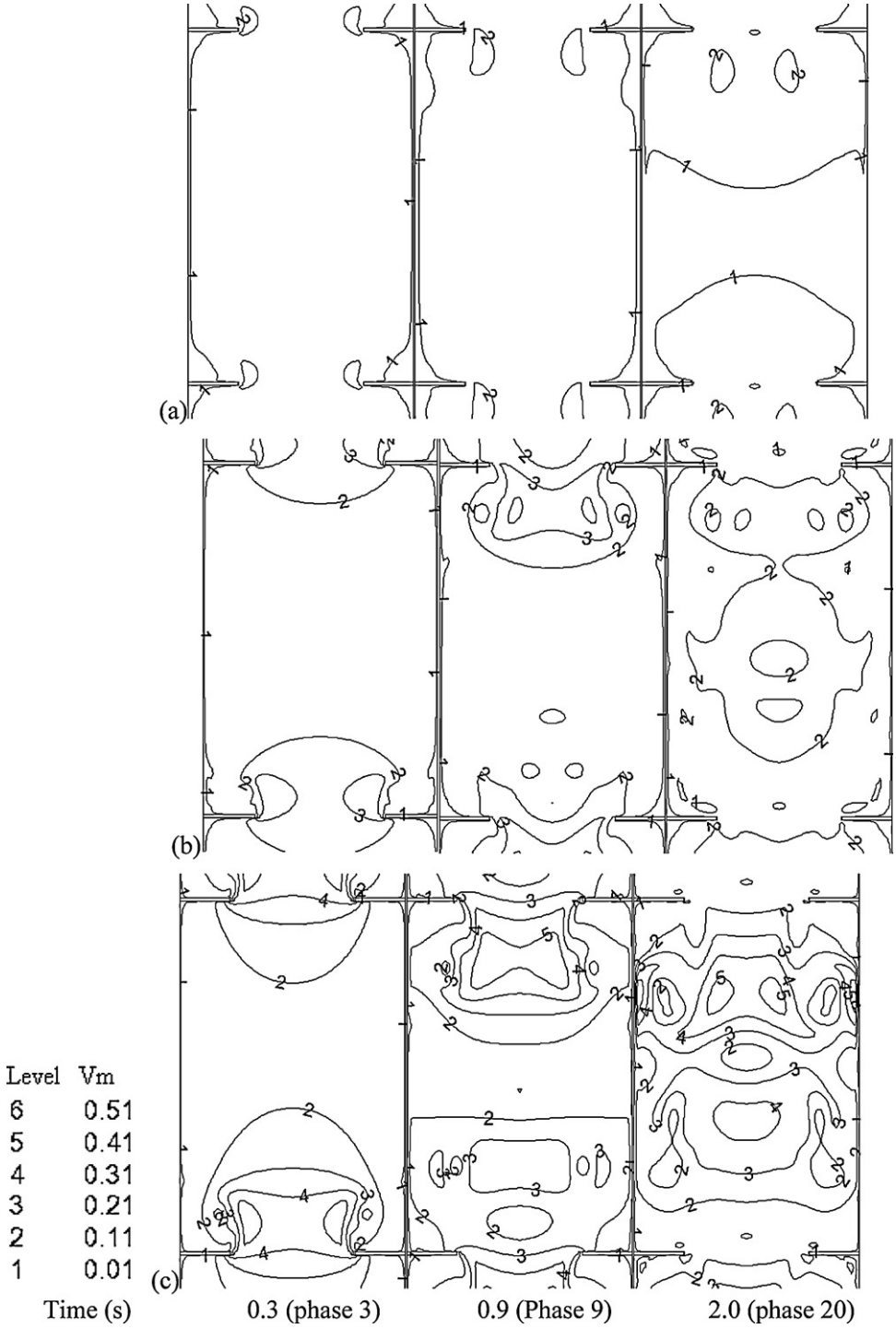

Fig. 4 – Velocity contour map with time at (a) $x_o = 5$ mm, (b) $x_o = 10$ mm, (c) $x_o = 15$ mm.

Momentum equations:

$$\rho\left(\frac{\partial V_r}{\partial t}+V_r\frac{\partial V_r}{\partial r}+\frac{V_\theta}{r}\frac{\partial V_r}{\partial \theta}-\frac{V_\theta{}^2}{r}+V_Z\frac{\partial V_r}{\partial z}\right)$$
$$=-\frac{\partial p}{\partial r}-\left[\frac{1}{r}\frac{\partial}{\partial r}(r\tau_{rr})+\frac{1}{r}\frac{\partial \tau_{r\theta}}{\partial \theta}-\frac{\tau_{\theta\theta}}{r}+\frac{\partial \tau_{rz}}{\partial z}\right] \quad (2)$$

$$\rho\left(\frac{\partial V_\theta}{\partial t}+V_r\frac{\partial V_\theta}{\partial r}+\frac{V_\theta}{r}\frac{\partial V_\theta}{\partial \theta}+\frac{V_rV_\theta}{r}+V_Z\frac{\partial V_\theta}{\partial z}\right)$$
$$=-\frac{1}{r}\frac{\partial p}{\partial \theta}-\left[\frac{1}{r^2}\frac{\partial}{\partial r}(r^2\tau_{r\theta})+\frac{1}{r}\frac{\partial \tau_{\theta\theta}}{\partial \theta}+\frac{\partial \tau_{\theta z}}{\partial z}\right] \quad (3)$$

$$\rho\left(\frac{\partial V_z}{\partial t}+V_r\frac{\partial V_z}{\partial r}+\frac{V_\theta}{r}\frac{\partial V_z}{\partial \theta}+V_Z\frac{\partial V_z}{\partial z}\right)$$
$$=-\frac{\partial p}{\partial z}-\left[\frac{1}{r}\frac{\partial}{\partial r}(r\tau_{rz})+\frac{1}{r}\frac{\partial \tau_{z\theta}}{\partial \theta}+\frac{\partial \tau_{zz}}{\partial z}\right] \quad (4)$$

where

$$\tau_{rr}=-\mu\left[2\frac{\partial V_r}{\partial r}-\frac{2}{3}(\nabla V)\right] \quad (5)$$

$$\tau_{\theta\theta}=-\mu\left[2\left[\frac{1}{r}\frac{\partial V_\theta}{\partial \theta}+\frac{V_r}{r}\right]-\frac{2}{3}(\nabla V)\right] \quad (6)$$

$$\tau_{zz} = -\mu\left[2\frac{\partial V_z}{\partial z} - \frac{2}{3}(\nabla V)\right] \quad (7)$$

$$\tau_{r\theta} = \tau_{\theta r} = -\mu\left[\frac{1}{r}\frac{\partial V_r}{\partial \theta} + r\frac{\partial}{\partial r}\left(\frac{V_\theta}{r}\right)\right] \quad (8)$$

$$\tau_{z\theta} = \tau_{\theta z} = -\mu\left[\frac{1}{r}\frac{\partial V_z}{\partial \theta} + \left(\frac{\partial V_z}{\partial z}\right)\right] \quad (9)$$

$$\tau_{zr} = \tau_{rz} = -\mu\left[\frac{\partial V_z}{\partial r} + \left(\frac{\partial V_r}{\partial z}\right)\right] \quad (10)$$

$$(\nabla V) = \frac{1}{r}\frac{\partial}{\partial r}(rV_r) + \frac{1}{r}\frac{\partial V_\theta}{\partial \theta} + \frac{\partial V_z}{\partial z} \quad (11)$$

To satisfy the oscillation flow in an OBC, oscillatory and periodic boundary conditions were used. A meshed 3-D domain with two orifice baffles is shown in Fig. 2 for all simulations. The column is 145 mm in diameter and 500 mm in length. The orifice diameter is 81 mm with spacing of 217.5 mm. The working fluid is water at a room temperature (density 998.2 kg/m^3, viscosity 0.001003 kg/ms). A complete hexahedral mesh was generated by Gambit 2.4.6. Table 1 displays the operating conditions used in the all simulations. The test cases with the boundary conditions on the bottom piston are shown in Fig. 3a. Analysis will be focused on four points as shown in Fig. 3b.

The numerical modeling procedures involved solving the governing equations using the pressure based solver and under-relaxation was used to control the change of scalar variables. In discretisation, a second order scheme for pressure momentum was used. The SIMPLEC algorithm was introduced in the pressure–velocity coupling scheme.

3. Results and discussion

Fig. 4 shows the velocity contours at three real time (0.3, 0.9 and 2.0 s) for case 1 (Fig. 4a), case 2 (Fig. 4b) and case 3 (Fig. 4c). For each case condition, refer to Table 1. Fig. 4a is a validation showing the same oscillation imposed at the piston. There is no phase angle lag on those specified points meaning that the imposed boundary is working without any error. The hexagonal mesh of 341,300 (mesh3) is grid independent solution and Fig. 6a shows that Mesh3 has reached at matured stage of refinement and further mesh refinement is not necessary.

A full cycle of 2 s has been divided into 20 equal time phase (of point 0.2 s) for clarity. The first phase represents the upstroke (phase 3 in Fig. 4), second one is at the end of downstroke oscillation (phase 9 in Fig. 4) and last one is full cycle at 2 s (phase 20 in Fig. 4). The dependence of the flow patterns on fluid oscillation amplitude was observed to differ for different oscillation amplitudes. Flow pattern developed for all oscillation amplitudes shows symmetric behavior (Fig. 4) for $Re_o < 250$ (Table 1). This kind of pattern is known as a soft mixing (Stonestreet and Van Der Veeken, 1999).

Table 1 – Working conditions for the 3D unsteady laminar simulations (hexagonal mesh of 341,300).

Case study	Case 1	Case 2	Case 3
Oscillation amplitude (mm)	5	10	15
Oscillation frequency (Hz)	1	1	1
$x_o f$ (mm/s)	5	10	15
Re_o	63	125	188
S_t	0.03	0.02	0.01
Time step size	0.001	0.001	0.001

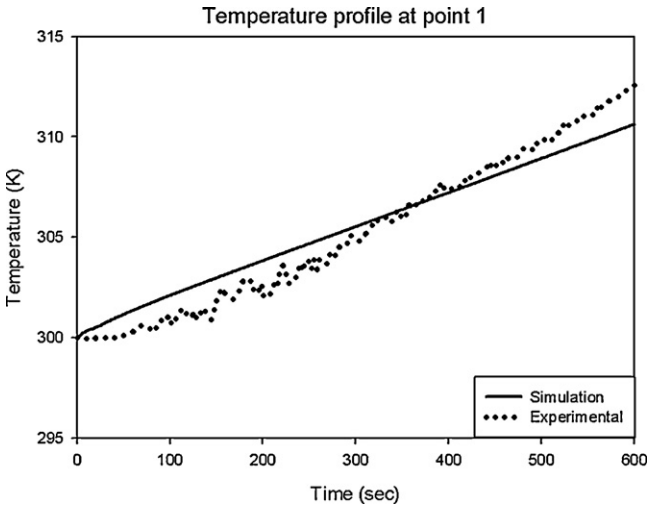

Fig. 5 – Comparison of numerical simulation and experimental work for temperature profile.

The velocity measurement was difficult for this case and only temperature was measured. Fig. 5 was obtained a comparison made between experimental works and numerical simulation for 600 s at point 1. In this period, temperature differences were found to be less than 0.70%. The greatest temperature differences occurred at t = 204 s which is about 0.66%. It shows CFD model can predict the temperature reasonably accurately for a long period of simulations and experimental works. Good prediction of numerical simulations using clamped heaters with OBC enables further studies using other parameters. In this work, efficiency of piston heater as additional heating agent in OBC can be explored numerically before the manufacturing of the real model would be wise option and cost saving. The detail of this test case can be found from the author's other publications.

Figs. 5a, b and 6a, b show a comparison of axial velocity distributions on different points (Fig. 3b) with varying amplitude in an oscillation cycle (cases 1–3). Oscillation cycle in accordance with sinusoidal graph for every point represents the periodic velocity boundary conditions is functional with user defined function. These results indicate the axial velocity increases with oscillation amplitude. For the case 1, maximum axial velocity for four points is around 0.11 m/s (Fig. 7b). When the oscillation amplitude is increased to 10 mm on case 2, the maximum velocity for axial component increased to 0.25 m/s (Fig. 6a). For the highest oscillatory Reynolds number which means case 3, the maximum axial velocity is 0.4 m/s (Fig. 6a and b).

In Figs. 8a, b and 9a, b the relationship between radial velocity and oscillation amplitude at various points (Fig. 3b) over oscillation cycle are shown. For all cases, the radial velocity component is quite small compared to the axial velocity produced by displacement of piston. The radial velocities at points 2 and 3 are higher than those at points 1 and 4. At the start of the upstroke, vortices begin to form and as the flow decelerates, the vortices are swept into the bulk of the column. At this time, downstroke vortices will collide with upstroke vortices at the middle of the column thereby increasing the radial velocity (Takriff, 2006). So, at points 2 and 3, a higher radial velocity is observed compare to both of points 1 and 4. Similar results also can be found in Oliveira and Ni (2001).

Fig. 10 shows vortices length with time for different oscillation amplitudes. Oscillations cycles are similar for the three cases but a different length of vortices formed. Turbulent

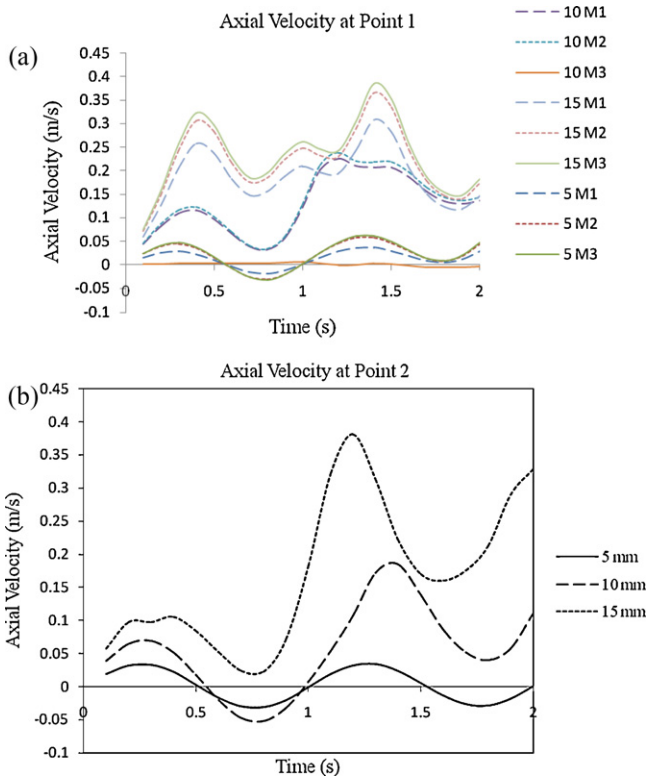

Fig. 6 – Axial velocity distributions with time step (a) point 1 and (b) point 2.

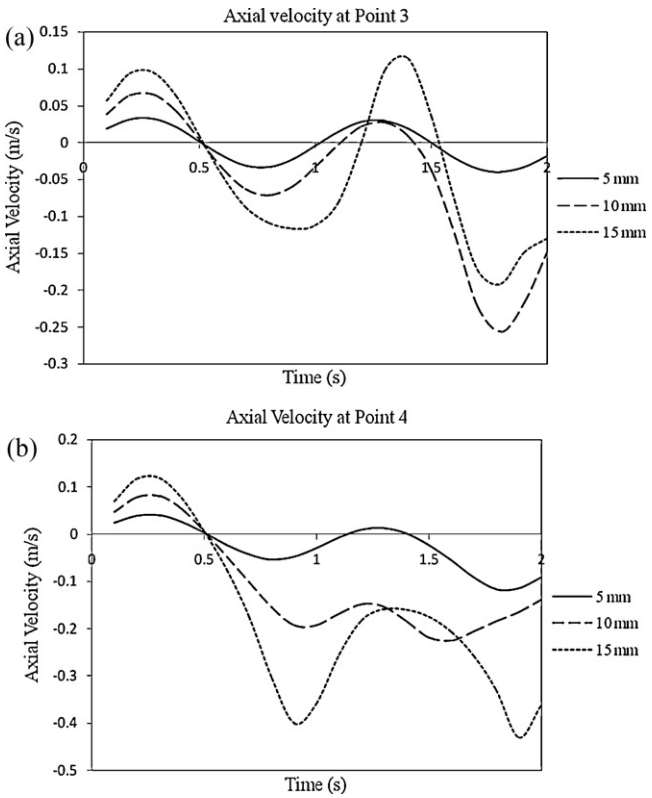

Fig. 7 – Axial velocity distributions with time step (a) point 3 and (b) point 4.

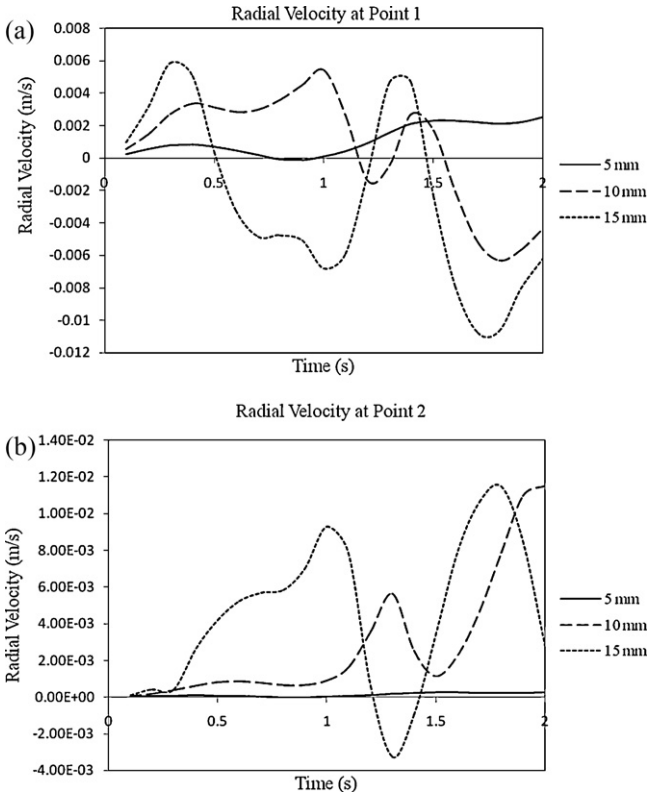

Fig. 8 – Radial velocity distributions with time step (a) point 1 and (b) point 2.

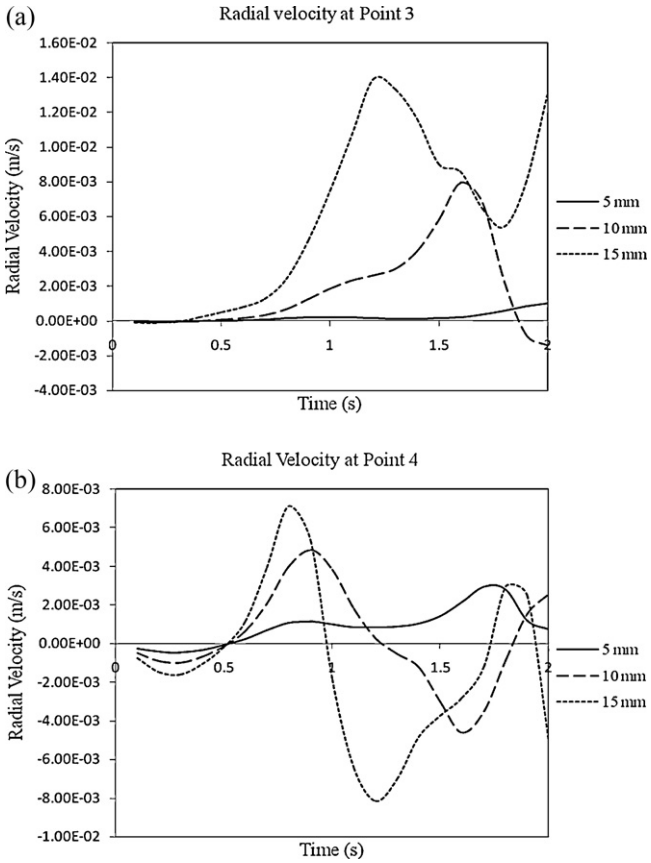

Fig. 9 – Radial velocity distributions with time step (a) point 3 and (b) point 4.

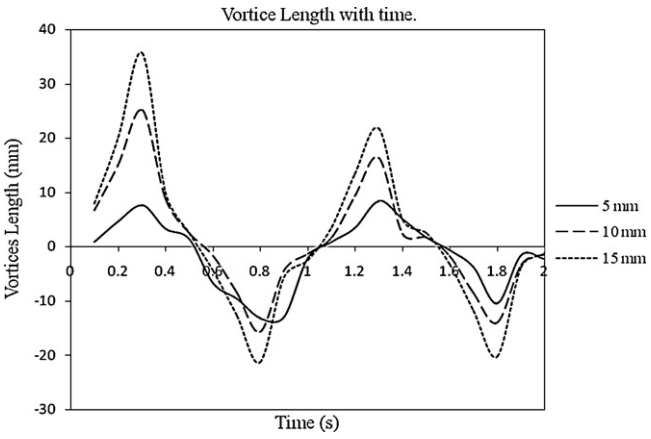

Fig. 10 – Vortices length average for different oscillation amplitudes over oscillation cycles at 2 s.

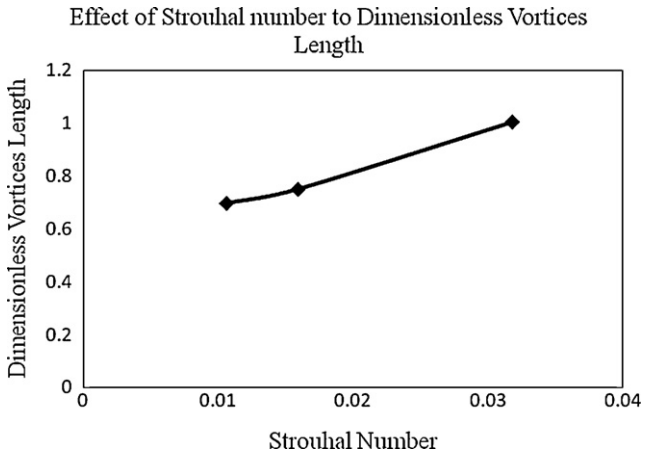

Fig. 11 – Effect of Strouhal number to dimensionless vortices length.

flows are characterized by vortices ranging in size from the integral length scale down to the Kolmogorov scale. The two ends of the range of vortex scales are associated with mixing behavior of fluid. For example, large-scale vortices account for most of the turbulent energy, while the small scales carry almost the entire vorticity and that is why the vortex length is important to know. For case 1, maximum vortices were formed around 14 mm. Nearly 25 mm length of vortices is formed for case 2. And the higher vortices length is 36 mm when oscillation amplitude is 15 mm (case 3). This results mean oscillation amplitude controls the length of vortices propagation. For higher oscillation amplitude, liquid will be carried further into the column from fitted baffle. This condition increases the axial velocity distributions.

The nondimentional amplitude of the oscillation is usually expressed as a function of Strouhal number. In Fig. 11, a dimensionless vortices average length is plotted against the Strouhal number. Vortex average length is normalised by corresponding oscillation amplitude. The dimensionless vortices average length of the oscillation increases with increasing Strouhal number.

4. Conclusions

Numerical study on the effect of oscillation amplitude to recirculation length in an oscillatory baffled column is presented. The results demonstrate, the maximum velocity for 5 mm, 10 mm and 15 mm in an OBC is 0.11 m/s, 0.25 m/s and 0.40 m/s respectively in the first cycle of oscillation. Vortex length was 1.5 times bigger when oscillation amplitude changes from 5 mm to 10 mm and 2 times when the amplitude is triple from 5 mm. A new relationship between Strouhal number with dimensionless vortices length was obtained. It was found that dimensionless vortices average length of the oscillation increases with increasing Strouhal number.

Acknowledgments

The authors wish to thank to National University of Malaysia for funding this project under grand number GUP-BTT-07-28-167. The author would also like to thank Petronas Technology University for assistance in preparing accommodation.

References

Fabiyi, M.E., Skelton, R.L., 1999. The application of oscillatory flow mixing to photocatalytic wet oxidation. Journal of Photochemistry and Photobiology A: Chemistry 129, 17–24.

Fitch, A.W., Jian, H., Ni, X., 2005. An investigation of the effect of viscosity on mixing in an oscillatory baffled column using digital particle image velocimetry and computational fluid dynamics simulation. Chemical Engineering Journal 112, 197–210.

Fluent, 2006. Fluent 6.3.

Gao, P., Han Ching, W., Herrmann, M., Kwong Chan, C., Yue, P.L., 2003. Photooxidation of a model pollutant in an oscillatory flow reactor with baffles. Chemical Engineering Science 58, 1013–1020.

Jian, H., Ni, X., 2005. A numerical study on the scale-up behaviour in oscillatory baffled columns. Chemical Engineering Research and Design 83, 1163–1170.

Mackley, M.R., Stonestreet, P., 1995. Heat transfer and associated energy dissipation for oscillatory flow in baffled tubes. Chemical Engineering Science 50, 2211–2224.

Ni, X., Fitch, A., Jian, H., 2004. Numerical and experimental investigations into the effect of gap between baffle and wall on mixing in an oscillatory baffled column. International Journal of Chemical Reactor Engineering 2, 1–16.

Ni, X., Gough, P., 1997. On the discussion of the dimensionless groups governing oscillatory flow in a baffled tube. Chemical Engineering Science 52, 3209–3212.

Ni, X., Jian, H., Fitch, A., 2003a. Evaluation of turbulent integral length scale in an oscillatory baffled column using large eddy simulation and digital particle image velocimetry. Chemical Engineering Research and Design 81, 842–853.

Ni, X., Jian, H., Fitch, A.W., 2002a. Computational fluid dynamic modelling of flow patterns in an oscillatory baffled column. Chemical Engineering Science 57, 2849–2862.

Ni, X., Mackley, M.R., Harvey, A.P., Stonestreet, P., Baird, M.H.I., Rama Rao, N.V., 2003b. Mixing through oscillations and pulsations—a guide to achieving process enhancements in the chemical and process industries. Chemical Engineering Research and Design 81, 373–383.

Ni, X., Murray, K.R., Zhang, Y., Bennett, D., Howes, T., 2002b. Polymer product engineering utilising oscillatory baffled reactors. Powder Technology 124, 281–286.

Oliveira, M.S.N., Ni, X., 2001. Gas hold-up and bubble diameters in a gassed oscillatory baffled column. Chemical Engineering Science 56, 6143–6148.

Reis, N., Vicente, A.A., Teixeira, J.A., Mackley, M.R., 2004. Residence times and mixing of a novel continuous oscillatory flow screening reactor. Chemical Engineering Science 59, 4967–4974.

Stephens, G.G., Mackley, M.R., 2002. Heat transfer performance for batch oscillatory flow mixing. Experimental Thermal and Fluid Science 25, 583–594.
Stonestreet, P., Harvey, A.P., 2002. A mixing-based design methodology for continuous oscillatory flow reactors. Chemical Engineering Research and Design 80, 31–44.
Stonestreet, P., Van Der Veeken, P.M.J., 1999. The effects of oscillatory flow and bulk flow components on residence time distribution in baffled tube reactors. Chemical Engineering Research and Design 77, 671–684.
Takriff, M.S., 2006. Pencampuran Aliran Berayun. Universiti Kebangsaan Malaysia, Bangi.